NASA TECHNICAL MEMORANDUM

NASA TM X-71468

NASA TM X-71468

INITIAL RESULTS FROM THE NASA LEWIS BUMPY TORUS EXPERIMENT

by J. Reece Roth, Richard W. Richardson, and Glenn A. Gerdin
Lewis Research Center
Cleveland, Ohio 44135

TECHNICAL PAPER proposed for presentation at Annual Meeting of the Plasma Physics Division of the American Physical Society
Philadelphia, Pennsylvania, August 31 - November 3, 1973

INITIAL RESULTS FROM THE NASA LEWIS BUMPY TORUS EXPERIMENT

BY

J. REECE ROTH, RICHARD W. RICHARDSON*, AND GLENN A. GERDIN*

NASA LEWIS RESEARCH CENTER

CLEVELAND, OHIO 44135

E-7769

ABSTRACT

Initial results have been obtained from low power operation of the NASA Lewis Bumpy Torus experiment, in which a steady-state ion heating method based on the modified Penning discharge is applied in a bumpy torus confinement geometry. The magnet facility consists of 12 superconducting coils, each 19 cm i.d. and capable of 3.0 T, equally spaced in a toroidal array 1.52 m in major diameter. A 18 cm i.d. anode ring is located at each of the 12 midplanes and is maintained at high positive potentials by a dc power supply. Initial observations indicate electron temperatures from 10 to 150 eV, and ion kinetic temperatures from 200 eV to 1200 eV. Two modes of operation are observed, which depend on background pressure, and have different radial density profiles. Steady state neutron production has been observed. The ion heating process in the bumpy torus appears to parallel closely the mechanism observed when the modified Penning discharge was operated in a simple magnetic mirror field.

INTRODUCTION

The NASA Lewis Bumpy Torus Experiment consists of a steady-state ion

---

*NRC Resident Research Associate

heating mechanism based on the modified Penning discharge, operating in a bumpy torus magnetic field configuration. The bumpy torus configuration receives its name from the shape assumed by the confined plasma, and consists of a number of coils (12 for the Lewis facility) arranged as indicated schematically in figure 1. The plasma assumes the form of a toroidal ring, with bumps in the region of weak field between the coils. This confinement geometry, in the form used in the Lewis facility, was proposed by Gibson, Jordan, and Lauer (ref. 1), who later performed an extensive series of investigations of single particle motion relevant to this geometry (refs. 2-5). Somewhat later, Geller (refs. 6-7) operated a pulsed plasma source in a bumpy torus geometry, and reported near classical confinement of the afterglow plasma (ref. 7). Fanchenko, et al. (ref. 8) have investigated turbulent heating in a bumpy torus plasma, and recently Sprott (ref. 9), who is associated with the Oak Ridge group, has examined the effects of magnetic field errors on particle confinement in a bumpy torus.

The Bumpy Torus experiment at the NASA Lewis Research Center is part of a program of research into the problems of ion heating, high temperature plasma physics, and thermonuclear power production which are associated with space applications (refs. 10, 11). The Bumpy Torus experiment was preceded by approximately nine years of research and development on the modified Penning discharge, which was operated in a superconducting magnetic mirror facility (ref. 12). During these earlier investigations, an ion heating mechanism associated with the modified Penning discharge was experimentally explored and a consistent model was developed to describe the ion heating mechanism (ref. 13-16).

The general approach adopted for the NASA Lewis Bumpy Torus experiment

may be summarized by five major points. (1) The plasma is confined in the bumpy torus magnetic field configuration. The relative simplicity of the magnets and force bearing structure which is possible in this configuration is advantageous in space where mass and reliability are at a premium. (2) The Bumpy Torus experiment was designed for steady state operation of both the magnetic field and the plasma. (3) It was desired to advance the state-of-the-art in superconducting magnets and other areas of technology in parallel with understanding of the basic physical processes in the plasma. (4) Previous investigations on the modified Penning discharge (ref. 13-16) demonstrated that it is feasible to generate ions with a Maxwellian distribution and with kinetic temperatures of up to several kilovolts. In the Bumpy Torus, the primary emphasis is on understanding this unique ion heating process, although achieving high densities and confinement times are also major goals. (5) An additional factor which distinguishes the NASA Lewis Bumpy Torus experiment from other approaches to controlled fusion is that a large positive potential is applied to the anode ring, forming a strong, inward directed radial electric field. This electric field plays an important role in the heating, and possibly in the stability and confinement of the plasma.

DESCRIPTION OF THE NASA LEWIS BUMPY TORUS FACILITY

The characteristics and performance of the NASA Lewis superconducting bumpy torus magnet facility have been described elsewhere (ref. 17-18). The basic structure of the magnetic field in this facility is illustrated in figure 1. The magnet array consists of 12 superconducting coils equally spaced around a toroidal volume 1.52 meters in major diameter. Each coil has a minor diameter of 19 cm, and the maximum designed magnetic field on the magnetic

axis is 3.0 T. The minimum magnetic field on the magnetic axis between coils is 40 percent of the maximum magnetic field. The coil array is located in a single vacuum tank 2.6 meters in major diameter.

In figure 2 is shown an isometric cutaway drawing of the facility. There are 12 airlocked access ports on the top of the vacuum tank which are used to insert and withdraw the high voltage anode rings. There are twelve 25 cm diameter viewports in the equatorial plane of the torus, which permit visual and experimental access to the plasma volume. Twelve 16 cm diameter ports are spaced on a 1.52 m diameter circle on the bottom of the vacuum vessel, some of which are available for instrumental access to the plasma. In figure 3 is shown a photograph of the bumpy torus facility with the top removed from the vacuum tank. Evident in this photograph are the 12 superconducting coils, each with four spacer bars which support the forces exerted by adjacent coils. At the top of the vacuum tank are three 100 liter liquid helium reservoirs which supply the coil array. The opening of the 80 cm diameter diffusion pump is visible at the bottom of the vacuum tank, as are a few of the 16 cm diameter access ports. An exterior photograph of the bumpy torus magnet facility is shown in figure 4. At eye level are visible some of the glass view ports which permit visual and experimental access to the plasma volume.

The magnet facility has met and exceeded its magnetic field design goals, and has been extremely reliable in its operational performance (refs. 17, 18). Approval to construct the facility was obtained in December 1969, and the preliminary shakedown tests were completed on April 30, 1972. The final shakedown tests of the facility were completed on November 1, 1972, and the first plasma was generated in the facility on December 6, 1972. The very satisfactory reliability of the facility is exemplified by a five-week long

experimental program in July and August 1973, during which the facility operated for 24 working days.

The plasma-physical results presented in this report were obtained with a 40 kV, 1 amp dc power supply. This power supply restricted the range of performance parameters accessible to the plasma to that indicated in Table I, and did not allow more than about 10 kilowatts of power input into the plasma. A larger high voltage dc power supply, shown on figure 5, will go into operation shortly. This power supply consists of two independent modules which can be connected to produce either 100 kV at 10 amps or 50 kV at 20 amps, depending on the plasma impedance at the intended operating conditions. The NASA Lewis bumpy torus experiment will not reach the limits of its intended performance parameters until this larger power supply is in operation.

CHARACTERISTICS OF THE BUMPY TORUS PLASMA

A photograph of the bumpy torus plasma is shown in figure 6, which was taken through one of the 25 cm diameter glass viewports in the equatorial plane of the torus. The vertical element in the foreground is the near side of an 18 cm i.d. water-cooled anode ring located at the midplane of the plasma. The necking down of the plasma in the vicinity of the mirror coils to the right and left is evident. Also apparent is the thick sheath which exists between the inner diameter of the anode ring and the plasma itself. The plasma at the opposite diameter of the torus is visible to the left of the anode ring in the foreground. The excellent visual and experimental access to the plasma is illustrated in this photograph, and makes it possible to operate the plasma with less plasma-wall interaction than would exist in a completely enclosed plasma.

In these experiments, the background gas consists of deuterium, with an admixture of helium when spectroscopic data were being taken. The percentage of helium gas was varied, and it was found that the electron temperature was not sensitive to the fraction of helium mixed with the deuterium.

The range of independent and dependent plasma parameters measured thus far is indicated on Table I. The error associated with these parameters is less than about 15 percent, except for the absolute plasma number density, which may be in error by as much as a factor of four. The absolute number density was estimated for Table I by tying the spectroscopically determined relative electron number density to a measurement made at high number densities with a microwave interferometer. Because of the uncertainty associated with the procedure, the data in the subsequent discussion are presented in terms of relative electron number densities. The maximum ion kinetic temperatures and number densities listed in Table I are limited by arcing problems and the limitations of the presently available power supply, which are expected to be overcome by future development work and the new 50 kV, 20 amp power supply shown on figure 5.

A significant feature of the modified Penning discharge in the bumpy torus geometry is that it contains no incandescent, electron-emitting, or heated electrodes in contact with the plasma. Only the water-cooled anode rings can be said to be in direct contact with the plasma, and they are separated from it by the anode sheath. The electrical circuit to the power supply is completed by ions which diffuse radially to the grounded walls surrounding the plasma, rather than electrons emitted from a heated cathode. This distinguishes the modified Penning discharge from arcs or reflex discharges, in which a heated, electron-emitting cathode is in direct contact

with the plasma, and plays a necessary role in their operation.

Fluctuations of electrostatic potential and light intensity were measured with capacitive probes and photomultipliers, respectively. These probes were placed at two different azimuthal locations at the same minor radius to detect phenomena rotating about the magnetic axis. These probes were also placed at the same minor azimuth, but at two different locations on the major circumference of the torus, at adjacent and distant "bumps." It was found from the probe and photomultiplier data that coherent fluctuations existed in the plasma, and were dominated by a low frequency $m = 1$ rotation about the minor circumference of the plasma. The rotation occurred with frequencies that ranged from 10 to 150 kHz, and appeared to consist predominantly of a rotating spoke of ions in a narrow anode sheath. At lower plasma densities, below approximately $5X10^9/cm^3$, the spoke rotation seemed also to involve the bulk of the plasma. This rotation of the plasma was evident in the electrostatic potential waveforms from the capacitive probes and also in the light intensity detected by a collimated photomultiplier. Capacitive probes and collimated photomultipliers were located at several positions around the major circumference of the torus, and it was found that these rotating spokes were in phase around the torus. The second most intense coherent phenomenon in the plasma is a fast rotation, with megahertz frequencies, also around the minor circumference of the plasma. This appeared to be a rotating spoke of electrons. These two distinct rotating spokes appeared to be qualitatively similar to the rotating spokes of ions and electrons previously observed in the modified Penning discharge and described in references 14-16.

The bumpy torus plasma operated in two distinct modes, one of which was prevalent at lower pressures, below approximately $5X10^{-5}$ torr, and a second mode which was prevalent above that pressure. The physical processes responsible

for these two modes of operation are not understood at present and are the subject of continuing investigations. As a result of the spectroscopic investigations to be described below, it was found that the radial profiles of electron temperature and number density differed in a characteristic manner in the two modes of operation.

The remaining diagnostic investigations showed that the plasma behaved in a manner similar to that observed in the modified Penning discharge and described in references 14-16. The electrons were typically a factor of five to twenty lower in energy than the ions. The measured range of ion temperatures was approximately 200 eV to 1200 eV in this experiment, and the electron temperatures ranged from about 10 eV to 150 eV. The ion energy distribution function tended to best fit a single temperature Maxwellian at the higher magnetic field strengths. Langmuir probe curves taken in the periphery of the plasma indicated that the electron energy distribution function was approximately Maxwellian also. Operation with the small power supply, which was also used on the modified Penning discharge, enabled up to 10 kW of steady state dc power to be injected into the bumpy torus plasma. Under the highest ion densities and kinetic temperatures attainable with this power supply, a steady-state flux of neutrons from DD reactions was observed from the plasma. Further diagnostic results are covered in the following sections.

ION TEMPERATURE MEASUREMENTS IN THE BUMPY TORUS

A charge exchange neutral particle analyzer was used to measure the energy distribution function and kinetic temperature of the ions perpendicular to the toroidal magnetic field in the bumpy torus. The analyzer is a duplicate of that developed by Valckx at Fontenay-aux-Roses (ref. 19), and the data were

taken and reduced in the manner described previously in reference 16. In figure 7 is shown the experimental arrangement of the charge exchange neutral analyzer with respect to the bumpy torus plasma. The analyzer was aimed directly across the minor diameter of the plasma, in the magnetic field mid-plane between two coils. Charge exchange neutrals from the opposite diameter of the toroidal plasma were prevented from entering the analyzer by a baffle plate in the center hole of the torus.

Plasma ions which charge exchange with the background molecular netural deuterium are sampled by the analyzer. The long mean free path of the energetic neutral deuterium with respect to the distance to the analyzer makes possible direct sampling of the plasma. The position of the entrance slits of the analyzer restricts the charge exchange neutrals to those generated in a limited region of the plasma, a column about 1 cm high and 1 cm wide across the plasma diameter. Only ions moving perpendicular to the toroidal magnetic field are sampled. The energetic charge exchanged neutral atoms are then re-ionized by a nitrogen gas cell at 100 microns of pressure and analyzed by a set of 90^{o} electrostatic deflector plates. The geometry of these plates requires that a re-ionized particle have an energy of 10 times the voltage across the plates per unit charge, in order to be detected by the photomultiplier at the output of the electrostatic deflector plates. The photomultiplier detector counts individual particles and the signal is integrated and plotted as a function of energy on an xy recorder. From these raw data several corrections are made as described in reference 16, to convert the raw data to the ion energy distribution function. These distribution functions are then compared with the negative slope portion of a Maxwellian distribution by a least squares procedure to determine a best-fitting ion temperature. The

raw data below 2 kV are not used in the fit, because the re-ionization probability is not known with certainty below this energy.

The measurements give ion kinetic temperatures that range from 200 eV to 1200 eV. It was found that the ion energy distribution functions could be classified into four mutually exclusive descriptive categories, samples of which are illustrated in figure 8. In this figure a characteristic example of the ion energy distribution functions is shown for each category, along with the best-fitting Maxwellian, where this is appropriate. The most common distribution function best fits a single slope Maxwellian and was observed in 47 percent of the experimental runs. An example of the single slope Maxwellian is shown in figure 8a. The reduced data closely fit a Maxwellian distribution over four orders of magnitude in the relative number density, or more than 9 energy e-folding lengths in spite of the fact that the analyzer sampled ions across the entire diameter of the plasma.

The next most frequent type of distribution function was the two-slope distribution illustrated in figure 8b. These two-slope distribution functions were observed in approximately 21 percent of the experimental runs. Such a two-slope distribution could result either from the detector sampling the center and the sheath of the plasma, with each region of the plasma having a different characteristic temperature; or the higher temperature component could represent impurities (or possibly D_2^+) which are hotter because of their higher mass, since all ions have a constant EXB/B^2 drift velocity.

The third type of ion energy distribution function is the two-humped

distribution illustrated in figure 8c. Neither hump fits a drift-free Maxwellian distribution, and it is clear that under these conditions the plasma as a whole is far from equilibrium. This type of distribution function tended to occur at pressures above $3.5X10^{-5}$ torr, and at midplane magnetic fields less than 0.2 tesla. The second hump occurs at an energy approximately twice that of the first maximum. The plasma at these operating conditions could consist of a Maxwellian plasma with an ion temperature of about 200 eV rotating at a high EXB/B^2 drift velocity. The second hump may be due to D_2^+ rotating with the same drift velocity.

The final ion energy distribution is shown in figure 8d, and is dominated by a single very large peak at the anode voltage of the plasma. These peaks tend to occur at pressures below $3.5X10^{-5}$ torr and at midplane magnetic fields less than 0.2 tesla. In some cases peaks occur at one-half and three-fourths of the anode voltage. The peak at one-half the anode voltage could be due either to dissociation of D_2^+ in the plasma or of D_2^+ or neutral D_2 in the gas cell.

Two hundred seventy-seven individual experimental runs were taken at seven different magnetic field strengths. It was found that the relative proportion of each type of ion energy distribution function depended on the strength of themagnetic field. To illustrate this point, the percentage of the total number of runs at each magnetic field which fell into each of the four categories is listed in Table II and shown in figure 9. The same general range of anode voltages, anode currents, background neutral gas pressures, and other parameters were covered at each of the seven magnetic field strengths investigated, except that the data population at 2.96 tesla did not include data to as low a pressure as was investigated at the other magnetic fields.

Too much significance should not be placed on the exact values of the percentages at a given magnetic field strength, because these percentages depend to some extent upon the signal-to-noise ratio and the distribution of the experimental points in parameter space. However, the trends are significant. As the magnetic field increases, the percentage of cases in which the ion energy distribution function best fits a Maxwellian increases with magnetic field. This is fortunate, because it is desirable in fusion applications that the ions be as Maxwellian as possible, in order to reduce the number of reservoirs of free energy available to drive plasma instabilities.

SPECTROSCOPIC MEASUREMENTS

Spatially and time-averaged electron temperature and relative number density have been measured spectroscopically over a range of discharge operating conditions in the NASA Lewis bumpy torus plasma. The electron temperature is measured from the ratio of selected spectral line intensities from a small admixture of helium gas. Relative number densities are deduced from the helium spectral line intensities and measured electron temperature.

The spectroscopic measurements were made with a [illegible] 1.5 meter Fastie-Ebert spectrometer. A thin horizontal chord through the plasma perpendicular to the magnetic field was viewed through a beam rotator and imaging optics as shown in figure 10. The measurements were made at the magnet mirror midplane in the region between a set of double anode rings spaced 3 cm apart. Chords at different vertical positions were observed by translation of the lens perpendicular to the optical axis. A standard lamp was used to determine the spectral response of the entire system.

In order to observe the helium spectral lines a small amount of helium

was added to the background deuterium gas. A constant helium background pressure of $7X10^{-6}$ torr was used for most runs based on an ionization gauge factor of 5.55. The deuterium background pressure was varied between $10X10^{-6}$ torr and $8X10^{-5}$ torr based on a gauge factor of 2.65. A few runs were taken at deuterium pressures of 4 - $10X10^{-6}$ torr for which a helium background pressure of $5X10^{-6}$ torr of helium was used.

Electron temperatures are measured by the helium line ratio technique (ref. 20-21). This technique utilizes the marked difference in electron energy dependence of the optical cross section between the singlet and triplet series of helium and between the He II and the neutral helium lines. The intensity of a spectral line I_{jk} due to a transition $j \rightarrow k$ in the case of single step electron excitation and spontaneous decay is

$$I_{jk} \doteq n_o n_e \langle f_{jk}(v)\, v \rangle \sigma_{jk} \qquad (1)$$

where n_o and n_e are the neutral helium and electron number density respectively. The variable $f_{jk}(v)$ is the apparent optical cross section shape function normalized to its maximum and is a function of the electron velocity v. The angle brackets indicate an average over the assumed electron energy distribution function which is taken to be Maxwellian, and σ_{jk} is the maximum apparent optical cross section. The ratio of the intensity of two spectral lines, $I_{jk}/I_{\ell m}$, is independent of electron density and is a function of electron temperature if the shape functions $f_{jk}(v)$ and $f_{\ell m}(v)$ are dissimilar. Sovie (ref. 20) has suggested that transitions from the ^1S and ^3S states be used since the optical cross section for excitation to these states has been shown to be insensitive to neutral background pressure, and hence multistep processes involving neutrals which would invalidate

equation (1).

The excitation coefficients $\sigma_{jk}\langle f_{jh}(v)v\rangle$ and appropriate ratios as functions of electron temperature have been numerically computed up to an electron temperature of 200 eV for the 2^3P-5^3S (4121 Å), 2^3P-4^3S (4438 Å), 2^1P-4^1S (5048 Å), and 2^1P-5^1S (4438 Å) transitions of neutral helium using the shape functions of references 22-24. The He^+ 3-4 (4686 Å) transition excitation coefficient has been calculated using the shape functions of references 25-26. For all lines the maximum cross sections σ_{jk} of reference 21 were used.

The relative electron density can be determined from the measured electron temperature and the relation

$$n_e \sim \frac{I'_{jk}}{n_0\langle f_{jk}(v)v\rangle\sigma_{jk}} \qquad (2)$$

where I'_{jk} is the observed relative spectral line intensity. This is useful for determining radial density profiles and observing the change in density with operating conditions of the discharge.

Relative helium line intensities spatially averaged across a chord through the plasma 2 cm from the edge of the plasma have been measured while systematically varying discharge operating conditions. The 2^3P-5^3S (4121 Å) and 2^3P-4^3S (4713 Å) triplet series transitions and 2^1P-4^1S (5048 Å) and 2^1P-5^1S (4438 Å) singlet series transitions of neutral helium were observed as well as the 4686 Å line of He II under the higher electron temperature conditions. With the discharge operating at a fixed voltage and constant deuterium pressure, the spectrometer was manually peaked on each spectral line and the light intensity measured with the helium supply on and off, the

difference being the spectral line intensity. No change in the background light level was detectable between the helium on and off conditions and no pronounced deuterium or impurity lines interfered with the helium lines. A sample set of spectroscopic data at a set discharge operating condition is presented in figure 11 along with scans of the spectrum near the line with and without helium. The noise level for the chosen conditions is about average.

A raw data plot of the spatially averaged electron temperature versus anode voltage is shown in figure 12 for the range of magnetic fields and background pressures indicated. The plotted temperatures are the average of the temperatures measured from the different possible singlet to triplet spectral line ratios. Temperatures measured from ratios involving the 4686 Å line were not used in the average but were in fair agreement where available. A general trend is evident, in that the electron temperature tends to increase with anode voltage. Resolution of the data into separate functional dependences on anode voltage, background pressure, magnetic field, and other plasma parameters is a subject of continuing investigation.

Figure 13 is a raw data plot of relative number density versus anode current for different magnetic fields and background pressures. The plotted densities are an average of the densities computed from each spectral line and the average electron temperature. These data indicate that the anode current depends on the plasma number density in the manner $I_p \sim n_e^{1.6}$, with a weaker dependence on neutral gas pressure and magnetic field. Resolution of these functional dependences on plasma parameters is a matter of current investigation.

The cumulative probability plot in figure 14 compares the temperature measured by the ratio of the 5048 Å and 4713 Å line intensities with that

measured from the ratio of the 4438 Å and 4121 Å line intensities for all data sets. The plot indicates a normal distribution over the bulk of the data with the (5048/4438) data measuring 5 percent lower temperature on the average. The scatter between the two measurements represented by the relative standard deviation is ±16 percent.

In figure 15 are shown sample vertical scans of the 5048 Å helium line intensity where the horizontal scale is the vertical distance of the chord from the center of the discharge and the vertical scale is the relative line intensity. A vertical scan is shown for the low and high pressure operating mode of the discharge. Forty point Abel inversions (ref. 27) have been made of the vertical profiles for the various spectral lines for various operating conditions of the discharge. The effect of the nonaxisymmetry due to toroidal curvature has been neglected.

Radial profiles of electron temperatures and number density for the low and high pressure operating modes of the discharge are shown in figures 16 and 17. The high pressure mode operates with maximum density at the center of the discharge and a spatially uniform electron temperature. The low pressure mode has a maximum density near the anode ring and an electron temperature which is higher near the anode ring and decreases towards the plasma center.

CONCLUDING REMARKS

On figure 18 is shown the total dc power flowing into the plasma (equal to the anode voltage times the plasma current) as a function of anode current, I_p for a fixed maximum magnetic field of 2.4 tesla. On this graph the two distinct modes of operation show up quite clearly. On figure 19 is shown the dc plasma

resistance, obtained by dividing the anode current into the anode voltage, as a function of the anode current, also for a fixed maximum magnetic field of 2.4 tesla. The data correlate quite well, and fall into narrow bands over many orders of magnitude of these external parameters. These two distinct bands are associated with the two modes of operation of the plasma.

The modified Penning discharge ion heating scheme has been shown to work satisfactorily on a toroidal plasma. The ion kinetic temperatures observed in this investigation, from 200 to 1200 eV, are comparable with the ion kinetic temperatures observed in the modified Penning discharge under similar operating conditions. In this investigation a superconducting bumpy torus magnet facility has been shown to be capable of operating reliably for periods of up to five weeks, and to be capable of generating a magnetic field equal to its nominal design value of 3.0 tesla. An 82 liter steady state hot ion plasma can be generated by the application of high voltage dc electrical power. The present state of development is limited by the power supply available, and by arcing, which limits the voltage applied to the anode rings to less than 20 kV. (Anode voltages as high as 45 kV were used in the predecessor experiments on the modified Penning discharge.) Steady state neutron production from DD reactions has been observed in this plasma.

Future work on the NASA Lewis bumpy torus experiment will include bringing into operation the 50 kV 20 amp power supply and exploring the range of performance parameters made possible by the higher anode currents and plasma densities. Additional diagnostics are to be brought into operation, including a new microwave interferometer to measure the plasma number density, and various RF diagnostics to measure the spectrum of RF power. It is intended

to use the characteristics of the RF spectrum as diagnostic tools. For example, it is hoped to identify the peaks corresponding to the ion cyclotron and ion plasma frequencies and thereby obtain information about the charge species in the plasma and the number density of the plasma. Finally, we hope to obtain time-resolved profiles of the relative electron density and the electric field as a result of ion beam probing of the bumpy torus plasma.

FIGURE CAPTIONS

Description

Figure No.

1 Schematic drawing of the bumpy torus magnetic confinement geometry.

2 Isometric, cutaway drawing of the NASA Lewis bumpy torus magnet facility.

3 Photograph of the NASA Lewis bumpy torus magnet facility with the vacuum tank lid removed.

4 Exterior photograph of the NASA Lewis bumpy torus magnet facility, with plasma diagnostic equipment.

5 High voltage dc power supply to be used for ion heating with the modified Penning discharge. This supply consists of two 50 kV, 10 amp modules, which may be connected in series or parallel.

6 Photograph of the bumpy torus plasma taken on the equatorial plane of the torus. The plasma at the opposite diameter of the torus is visible to the left of the anode ring in the foreground.

7 Geometric arrangement, to scale, of the charge-exchange neutral analyzer.

8 Examples of four mutually exclusive types of ion energy distribution functions observed in the bumpy torus plasma operating at low power: (a) Maxwellian distribution; (b) two Maxwellian distributions, each at different kinetic temperatures; (c) two-humped, non-Maxwellian distribution function; and (d) non-Maxwellian distribution dominated by a single peak at an energy approximately equal to the anode voltage.

9 The percentage of ion energy distribution functions in each of the

four categories shown in figure 8, as a function of the magnetic field strength.

10 Schematic drawing of the spectroscopic apparatus used to take electron temperature, relative electron number density, and radial profiles of these quantities.

11 Example of typical spectral peak, background noise, and method of measuring the peak height.

12 Electron temperature as a function of anode voltage.

13 Anode current flowing to the plasma as a function of relative electron number density.

14 Cumulative probability plot of temperature ratios.

15 Raw data showing a radial scan of the amplitude of the 5048 Å helium line for the two operating modes of the discharge.

16 Radial profiles of relative electron number density for the two operating modes of the discharge.

17 Radial profile of the electron temperature for the two operating modes of the discharge.

18 The dc power flowing to the plasma, W_p, as a function of the anode current, I_p, for a population of data (not that shown in figure 17) taken at a fixed magnetic field of 2.4 T and at various pressures. The data fall into two distinct groups, corresponding to the high and low pressure modes of operation.

19 The dc plasma resistance, $R_p = V_a/I_p$, as a function of the current flowing to the plasma, I_p, for the same data population shown in figure 18. The data fall into two groups, corresponding to the high and low pressure modes of operation.

20

TABLE CAPTIONS

Table I Range of Experimental Parameters

Table II Number of ion energy spectra of each type at each magnetic field investigated.

REFERENCES

1. Gibson, G.; Jordan, W. C.; Lauer, E. J.: Bumpy Torus. Phys. Rev. Lett., vol. 4, no. 5, March 1, 1960, pp. 217-219.

2. Gibson, G.; Jordan, W. C.; Lauer, E. J.: Containment of Positrons in a Mirror Machine. Phys. Rev. Lett., vol. 5, no. 4, Aug. 15, 1960, pp. 141-144.

3. Gibson, G.; Jordan, W. C.; Lauer, E. J.: Particle Behavior in Static Axially Symmetric Magnetic Mirror and Cusp Geometries. Phys. Fluids, vol. 6, no. 1, Jan. 1963, pp. 116-133.

4. Gibson, G.; Jordan, W. C.; Lauer, E. J.: Particle Behavior in a Static, Asymmetric Magnetic Mirror Geometry. Phys. Fluids, vol. 6, no. 1, Jan. 1963, pp. 133-141.

5. Gibson, G.; Jordan. W. C.; Lauer, E. J.; Woods, C. H.: Guiding Center Motion and Plasma Behavior in the Bumpy Torus. Phys. Fluids, vol. 7, no. 4, April 1964, pp. 548-556.

6. Geller, R.: A Pulsed Toroidal P.I.G. Discharge. Applied Phys. Lett., vol. 2, no. 11, May 1, 1963, pp. 218-219.

7. Geller, R.: Experimental Results of a Bumpy Torus Discharge. Phys. Rev. Lett., vol. 10, no. 11, June 1, 1963, pp. 463-465.

8. Fanchenko, S. D.; Demidov, B. A.; Elagin, N. I.; Perepelkin, N. F.: Turbulent Plasma Heating in a Torus. Phys. Rev. Lett., vol. 21, no. 12, Sept. 16, 1968, pp. 789-791.

9. Sprott, J. C.: Effect of Magnetic Field Errors on Confinement in Bumpy Tori. Phys. Fluids, vol. 16, no. 7, July 1973, pp. 1157-1159.

10. Roth, J. R.; Rayle, W. D.; Reinmann, J. J.: Technological Problems Anticipated in the Application of Fusion Reactors to Space Propulsion

and Power Generation. NASA TM X-2106, Oct. 1970.

11. Roth, J. R.; Rayle, W. D.; Reinmann, J. J.: Fusion Power for Space Propulsion. New Scientist, April 20, 1972, pp. 125-127.

12. Roth, J.R.; Freeman, D. C.; Haid, D. A.: Superconducting Magnet Facility for Plasma Physics Research. RSI, vol. 36, no. 10, Oct. 1965, pp. 1481-1485.

13. Roth, J. R.: Experimental Study of Spectral Index, Mode Coupling, and Energy Cascading in a Turbulent, Hot-Ion Plasma. Phys. Fluids, vol. 14, no. 10, Oct. 1971, pp. 2193-2202.

14. Roth, J. R.: Origin of Hot Ions Observed in a Modified Penning Discharge. Phys. Fluids, vol. 16, no. 2, 1973, pp. 231-236.

15. Roth, J. R.: Hot Ion Production in a Modified Penning Discharge. IEEE Trans. on Plasma Sci., vol. 1, no. 1, 1973, pp. 34-45.

16. Roth, J. R.: Energy Distribution Functions of Kilovolt Ions in a Modified Penning Discharge. Plasma Physics, vol. 15, no. 10, 1973, pp. 995-1005.

17. Roth, J. R.; Holmes, A. D.; Keller, T. A.; and Krawczonek, W. M.: Characteristics and Performance of a 12-Coil Superconducting "Bumpy Torus" Magnet Facility for Plasma Research. NASA TN D-7353, Aug. 1973.

18. Roth, J. R.; Holmes, A. D.; Keller, T. A.; Krawczonek, W. M.: A 12-Coil Superconducting "Bumpy Torus" Magnet Facility for Plasma Research. IEEE Proc. of the 1972 Applied Superconductivity Conf., Annapolis, Md., May 1972, pp. 361-366.

19. Valckx, F. P. G.: Electrostatic Analyzer for the Detection of Fast Neutral Particles. EUR-CEA-FC-225, June 1964. Available as NASA TTF-11458, 1968.

20. Sovie, Ronald J.: Spectroscopic Determination of Electron Temperature and Percentage Ionization in a Helium Plasma. Physics Fluids, vol. 7, no. 4, April 1964, pp. 613-614.

21. Latimer, I.D.; Mills, J. I.; Day, R. A.: Refinements in the Helium Line Ratio Technicue for Electron Temperature Measurement and Its Application to the Precursor. J. Quant. Spectr. Rad. Trans., vol. 10, 1970, pp. 629-635.

22. Jobe, J. D.; St. John, R. M.; Absolute Measurements of the 2^1P and 2^3P Electron Excitation Cross Sections of Helium Atoms. Phys. Rev., vol. 164, no. 1, Dec. 5, 1967, pp. 119-121.

23. Latimer, I. D.: private communication.

24. Kay, R. B.; Showalter, J. G.; Exchange Excitation in Helium: Excitation Functions for the 4^3S, 3^3P, and 3^3D Levels. Phys. Rev. A., vol. 3, no. 6, June 1971, pp. 1998-2006.

25. St. John, R. M.; Lin, C.C.: Production of Excitation and Ionization in Helium by Single Electron Impact. J. Chem. Phys., vol. 41, no. 1, July 1, 1964, pp. 195-197.

26. Moussa, H. R. Moustafa: Physica, vol. 36, 1967, p. 646.

27. Lochte-Holtgreven, ed.: Plasma Diagnostics. North Holland Publishing Co., 1968, pp. 184-186.

TABLE I

RANGE OF EXPERIMENTALLY OBSERVED PARAMETERS

Quantity	High Value	Low Value
Anode Voltage, kV	20	1.0
Anode Current, mA	900	0.10
Input Power, Watts	7000	.080
Gas	- Deuterium -	
Maximum Magnetic Field, Tesla	3.0	0.24
Neutral Gas Pressure, Torr	$2.9X10^{-6}$	$9.1X10^{-5}$
Electron Kinetic Temperature, eV	150	10
Ion Kinetic Temperature, eV	1200	200
Electron Number Density/cm^3	$4X10^{10}$	10^9

TABLE II

ION ENERGY SPECTRA IN VARIOUS CATEGORIES

NOMINAL MAXIMUM MAGNETIC FIELD, TESLA	A SINGLE SLOPE DISTRIBUTION	B TWO-SLOPE DISTRIBUTION	C TWO HUMPED	D SINGLE PEAK	E MISC.	TOTAL
.239	4 (8.5%)	0	29 (61.7%)	14 (29.8%)	0	47
.478	1 (3.1%)	0	19 (59.4%)	12 (37.5%)	0	32
.955	14 (46.7%)	5 (16.7%)	5 (16.7%)	6 (20%)	0	30
1.43	18 (50%)	15 (41.7%)	3 (8.3%)	0	0	36
1.91	29 (66%)	14 (31.8%)	1 (2.3%)	0	0	44
2.39	45 (70.3%)	19 (29.7%)	0	0	0	64
2.96	18 (75%)	5 (20.8%)	1 (4.2%)	0	0	24
GRAND TOTAL	129 (46.5%)	58 (20.9%)	58 (20.9%)	32 (11.6%)	0	277

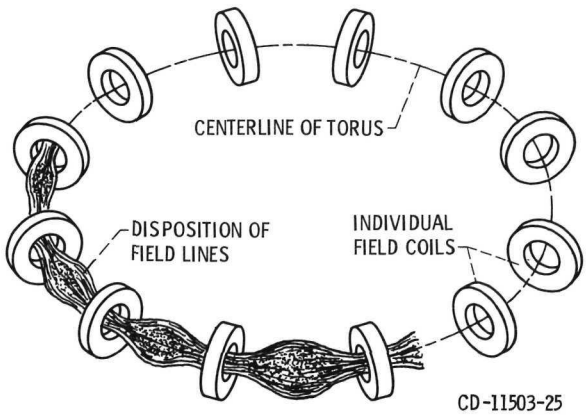

Figure 1. - Schematic drawing of the bumpy torus magnetic confinement geometry.

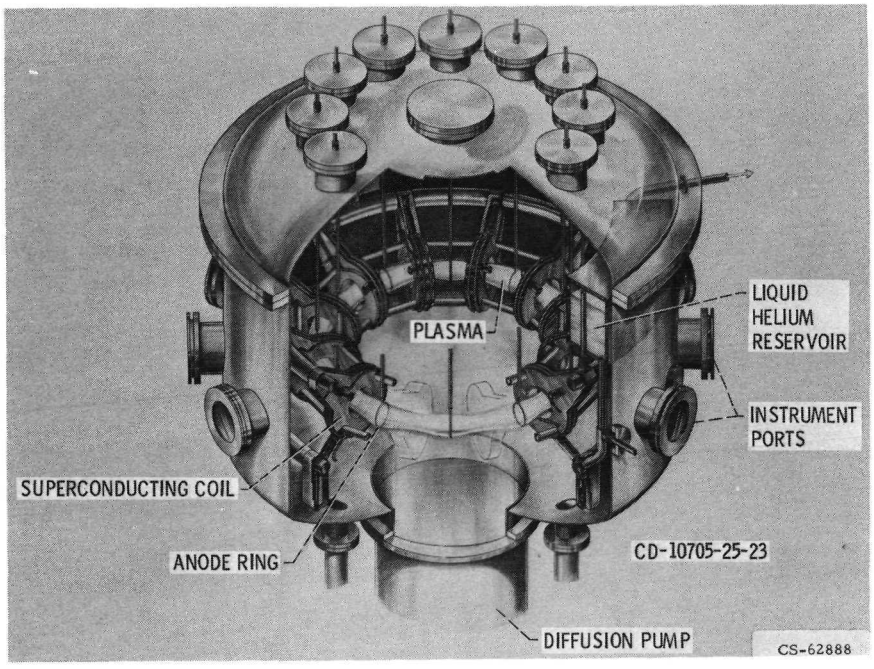

Figure 2. - Isometric, cutaway drawing of the NASA Lewis bumpy torus magnet facility.

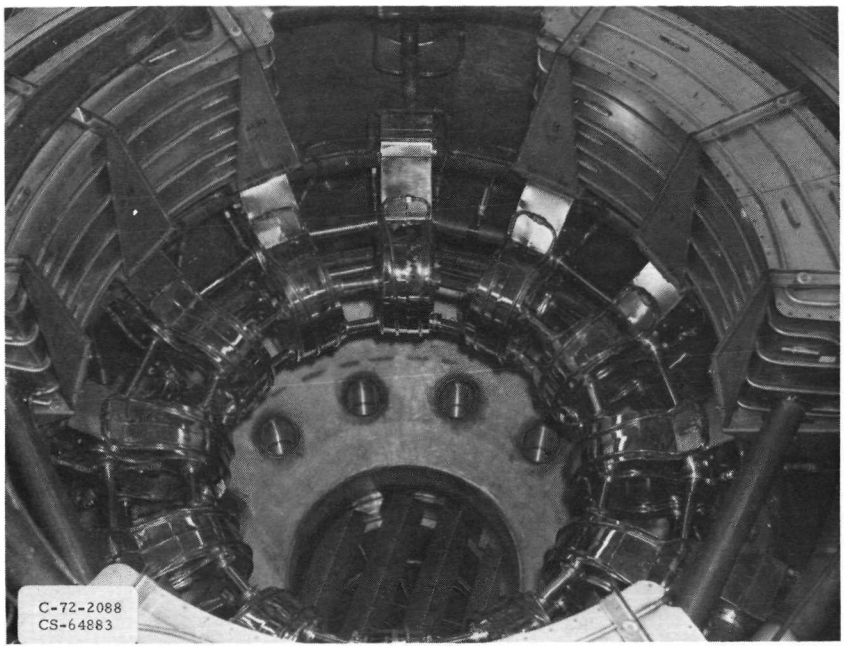

Figure 3. - Photograph of the NASA Lewis bumby torus magnet ficility with lid removed from vacuum tank.

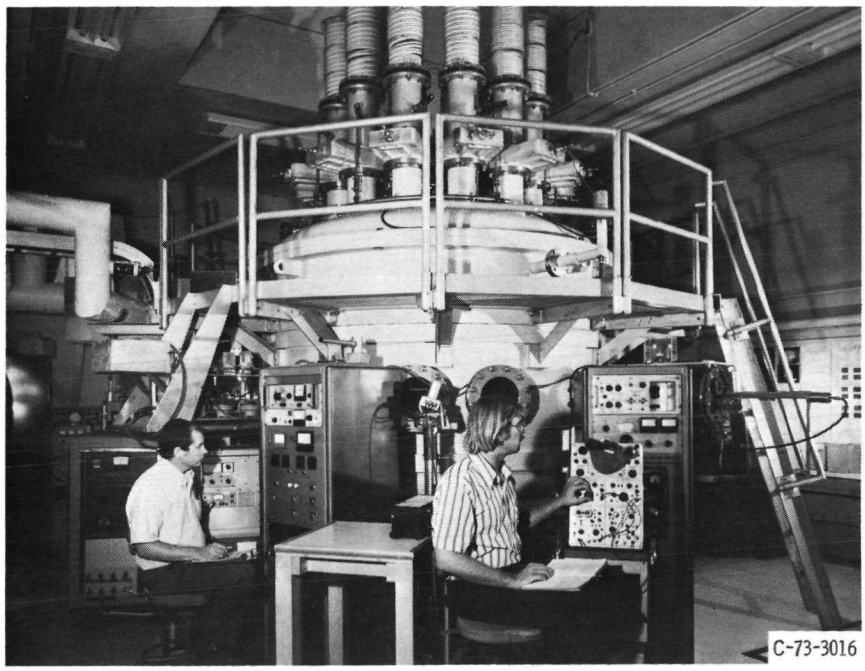

Figure 4. - Exterior photograph of the NASA Lewis bumpy torus magnet facility, with plasma diagnostic equipment.

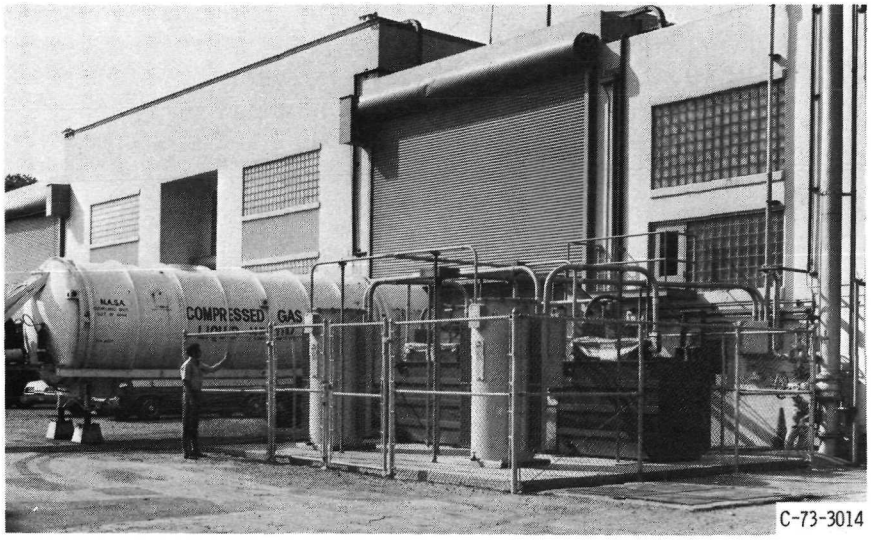

Figure 5. - High voltage dc power supply to be used for ion heating with the modified Penning discharge. This supply consists of two 50 kV, 10 amp modules, which may be connected in series or parallel.

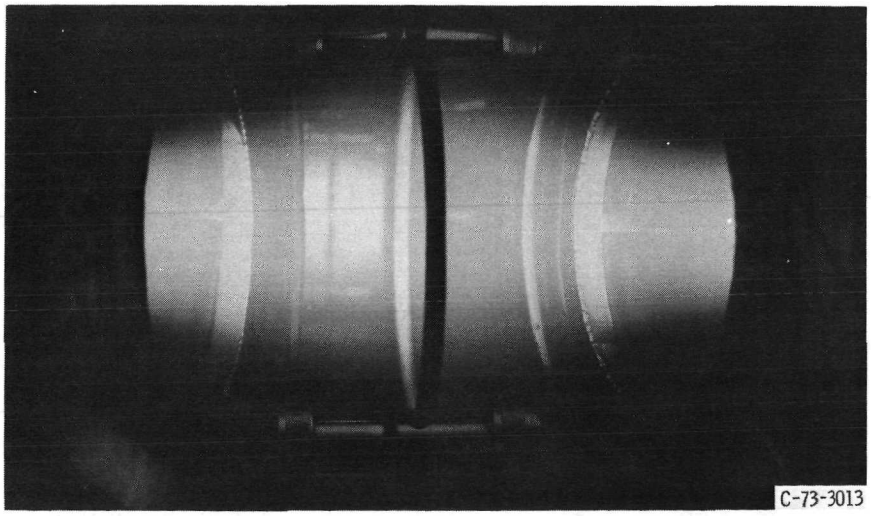

Figure 6. - Photograph of the bumby torus plasma taken on the equatorial plane of the torus. The plasma at the opposite diameter of the torus is visible to the left of the anode ring in the foreground.

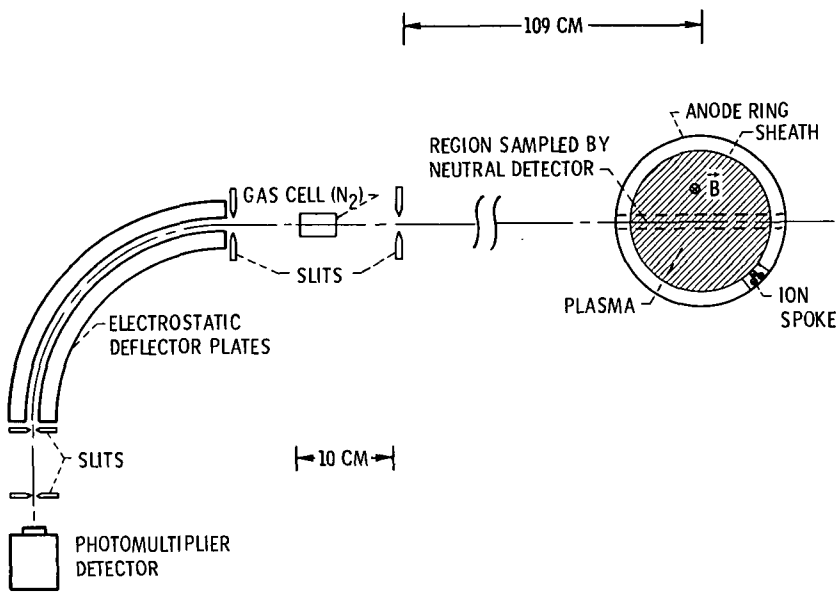

Figure 7. - Schematic drawing of the charge-exchange neutral detector. The line of sight of the detector was in the toroidal midplane and perpendicular to the axis of the torus.

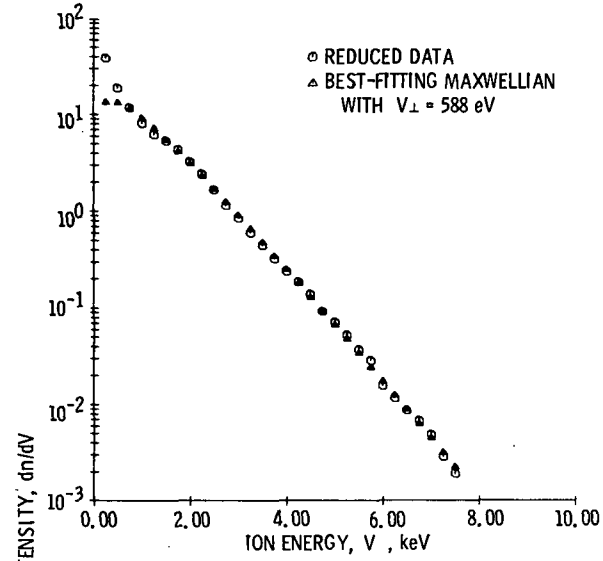

(a) MAXWELLIAN DISTRIBUTION, ANODE VOLTAGE V_A = 8 kV.

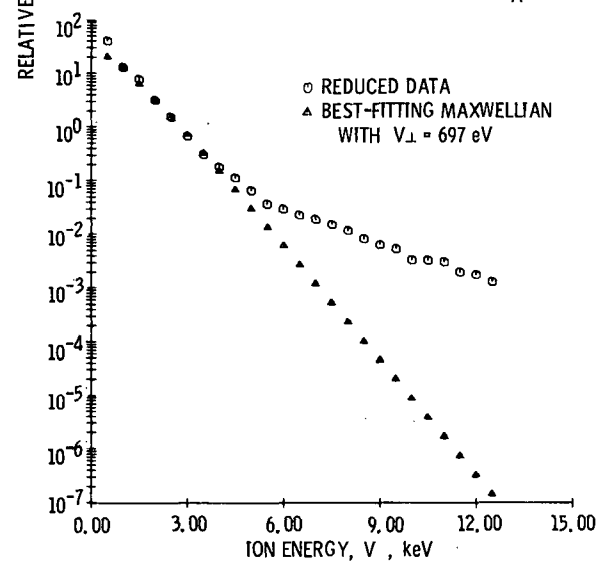

(b) TWO SLOPE DISTRIBUTIONS, ANODE VOLTAGE V_A = 12.5 kV.

Figure 8. - Examples of four mutually exclusive types of ion energy distribution functions observed in the bumpy torus plasma operating at low power.

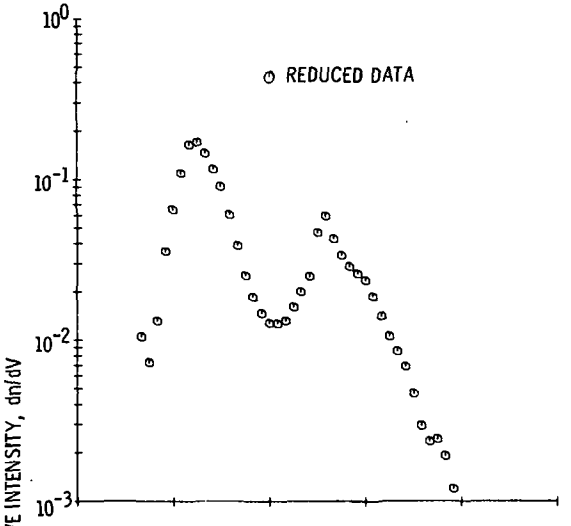

(c) TWO-HUMPED DISTRIBUTION, ANODE VOLTAGE V_A = 7.5 kV.

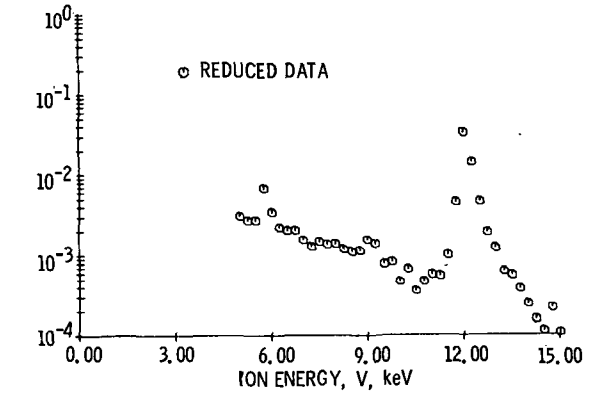

(d) PEAK-DOMINATED DISTRIBUTION, ANODE VOLTAGE V_A = 12.5 kV.

Figure 8. - Concluded.

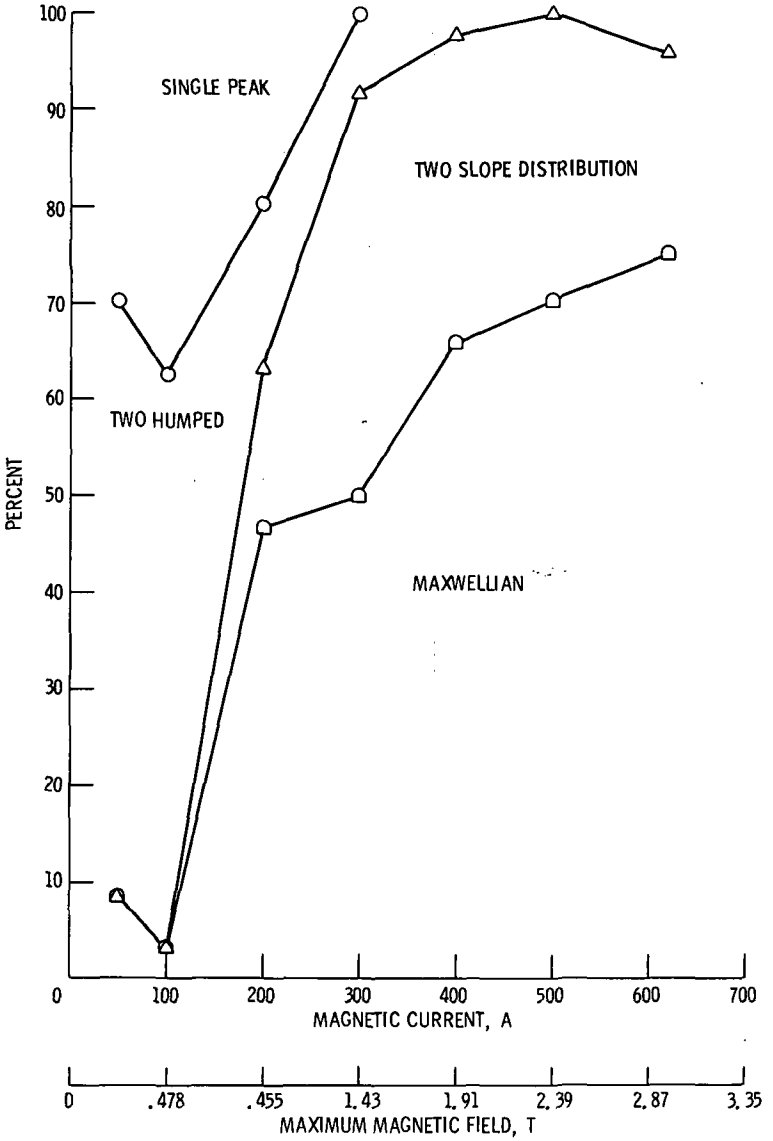

Figure 9. - The percentage of ion energy distribution functions in each of the four categories shown in figure 8, as a function of the magnetic field strength, and with a small admixture of helium gas.

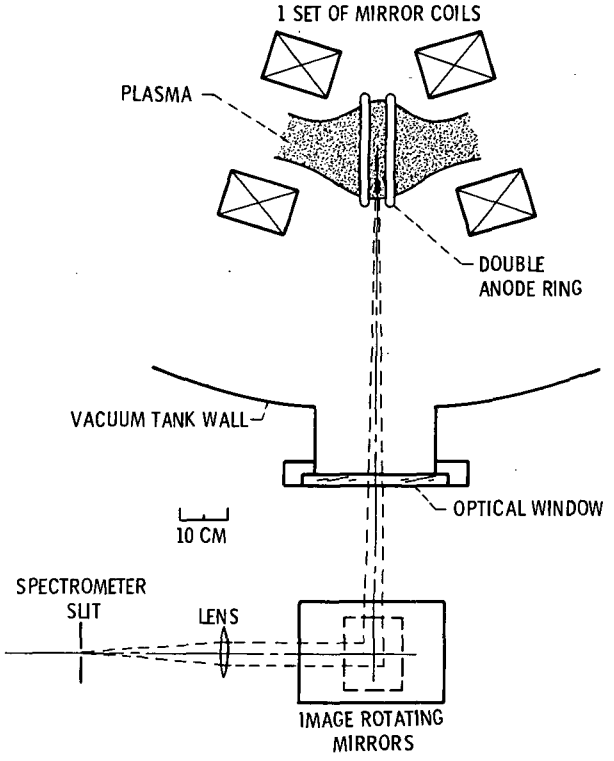

Figure 10. - Schematic drawing of the spectroscopic apparatus used to take electron temperature, relative electron number density, and radial profiles of these quantities.

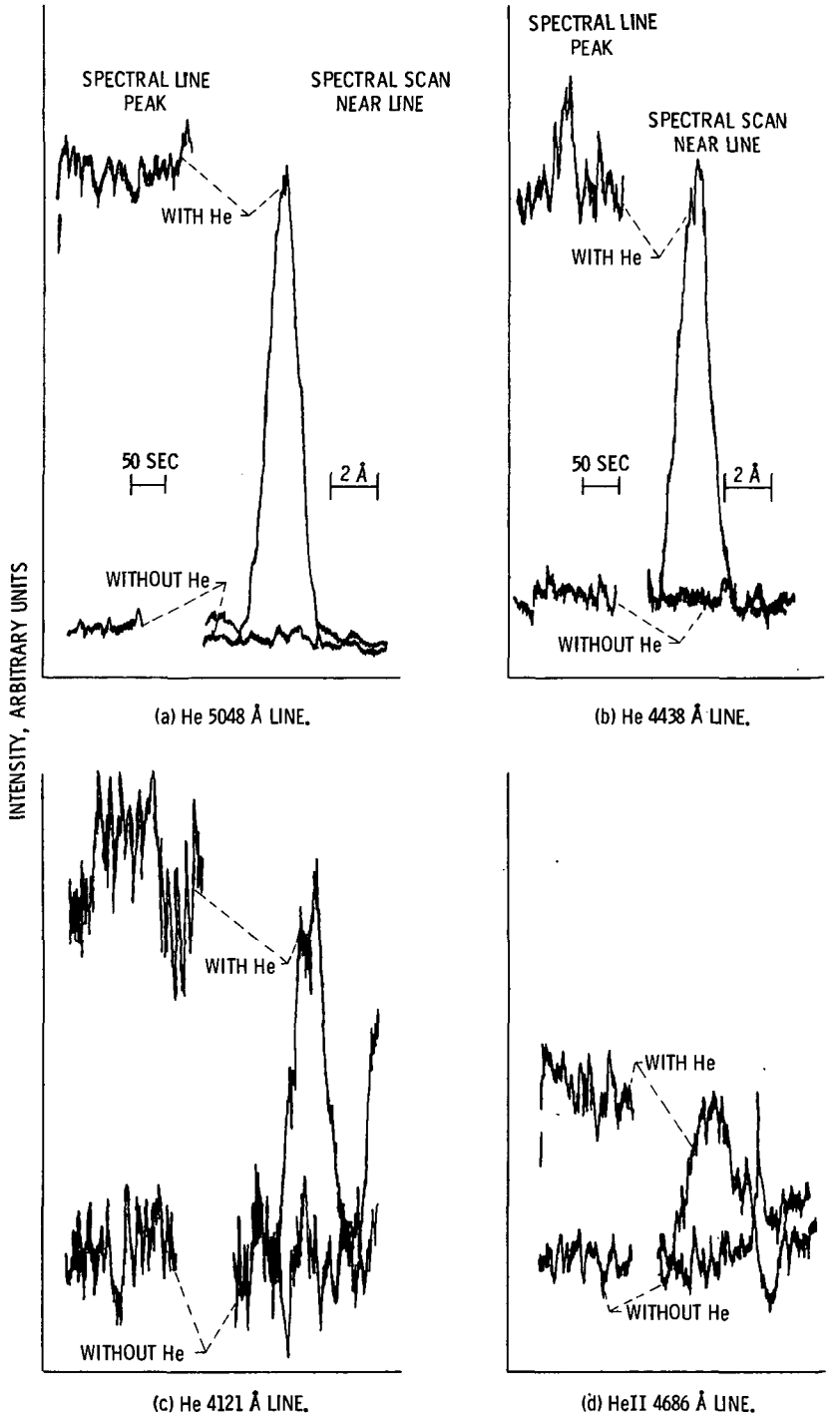

Figure 11. - Example of typical spectral peak, background noise, and method of measuring the peak height.

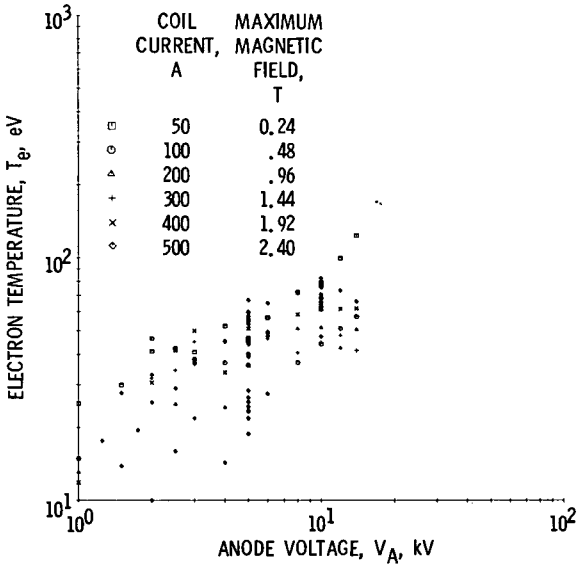

Figure 12. - Electron temperature as a function of anode voltage.

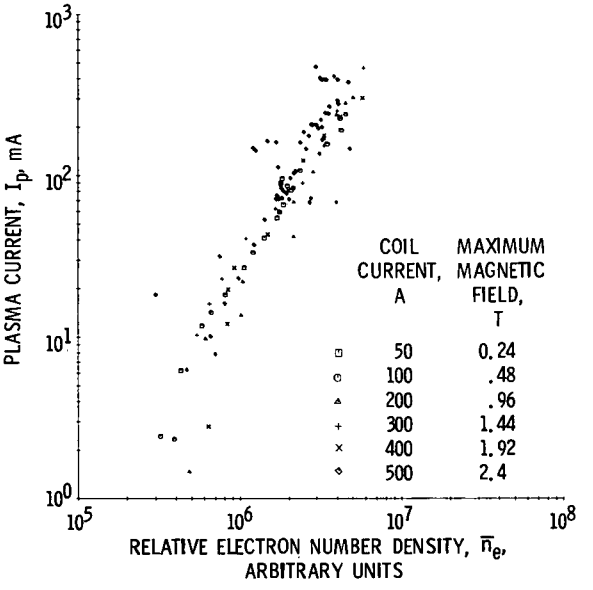

Figure 13. - Anode current flowing to the plasma as a function of relative electron number density.

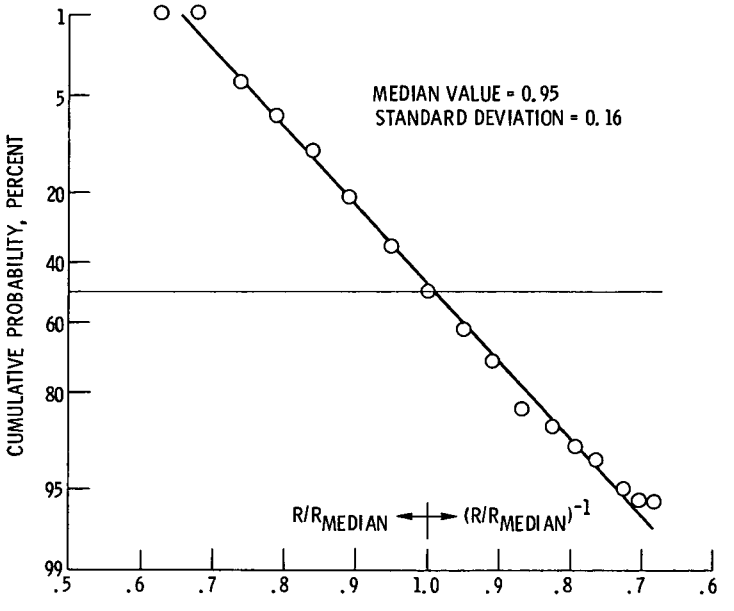

Figure 14. - Cumulative probability plot of R the ratio of the electron temperature measured by the 5048 Å and 4713 Å lines to that measured by the 4438 Å and 4121 Å lines for all data sets normalized to R median.

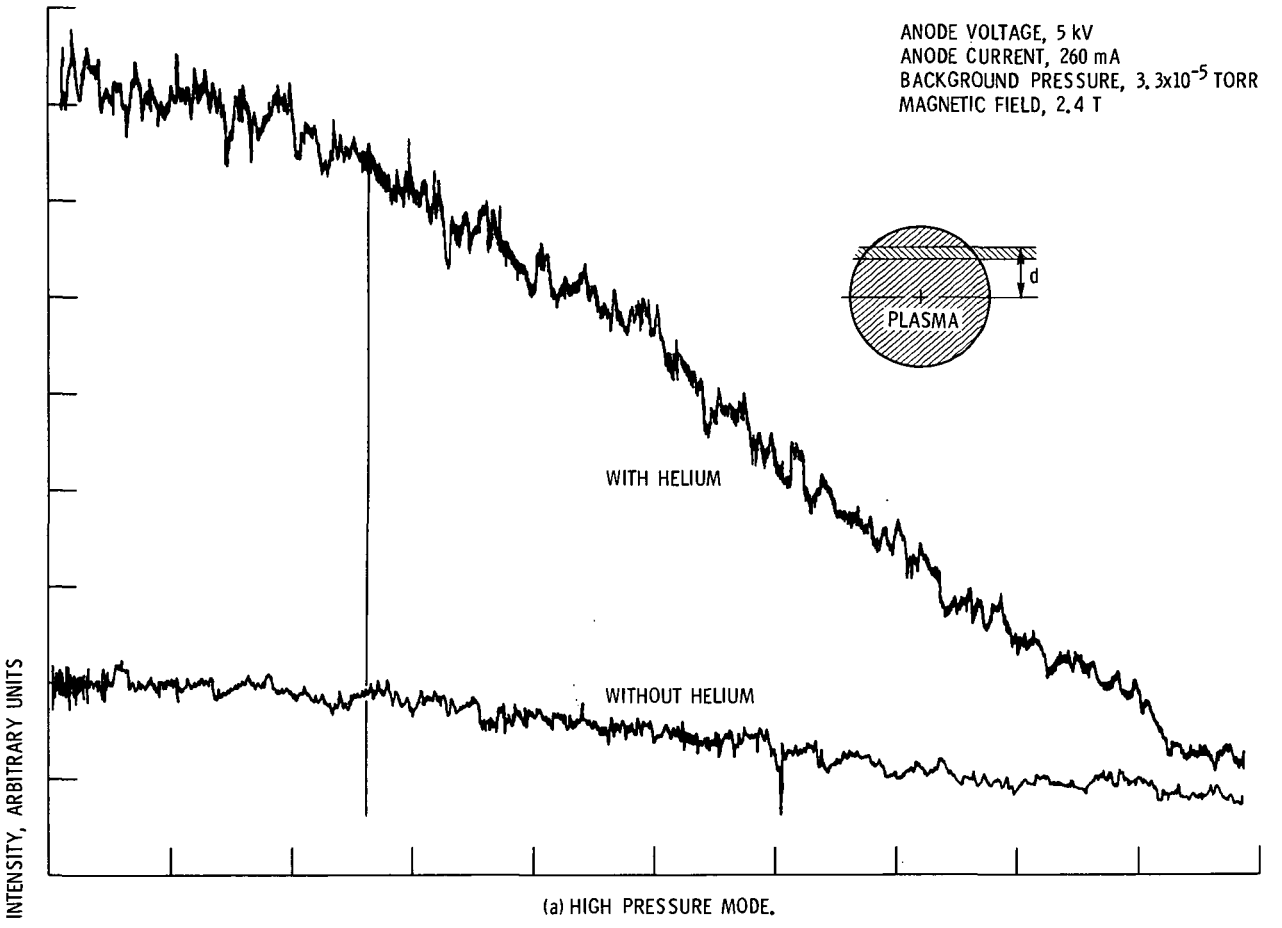

(a) HIGH PRESSURE MODE.

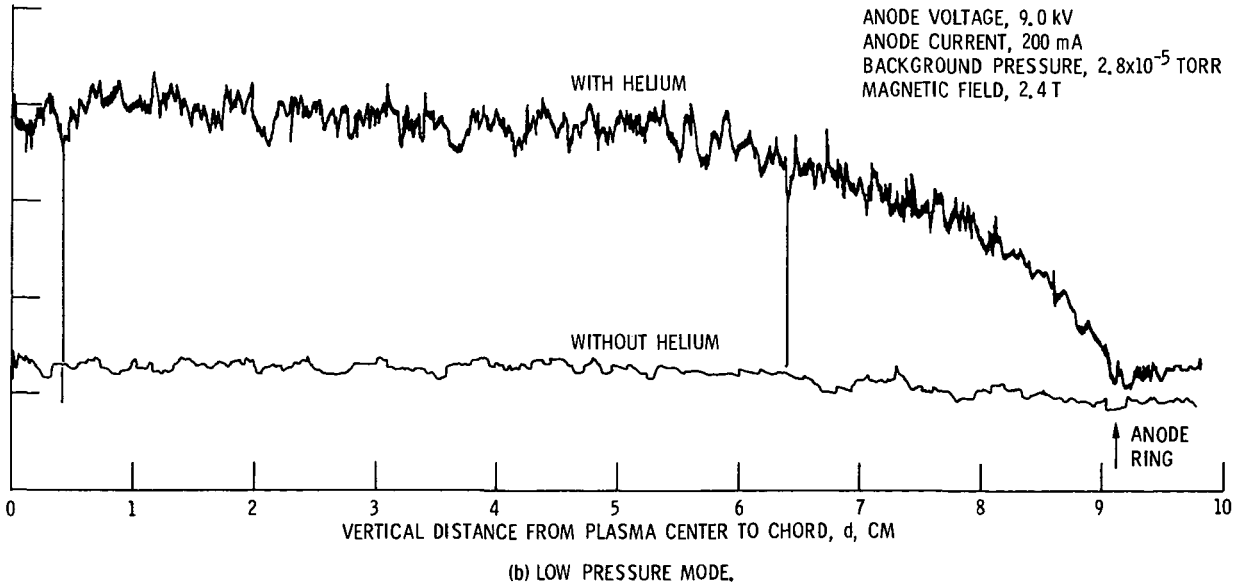

(b) LOW PRESSURE MODE.

Figure 15. - Raw data showing a vertical scan of the amplitude of the 5048 A helium line for the two operating modes of the discharge.

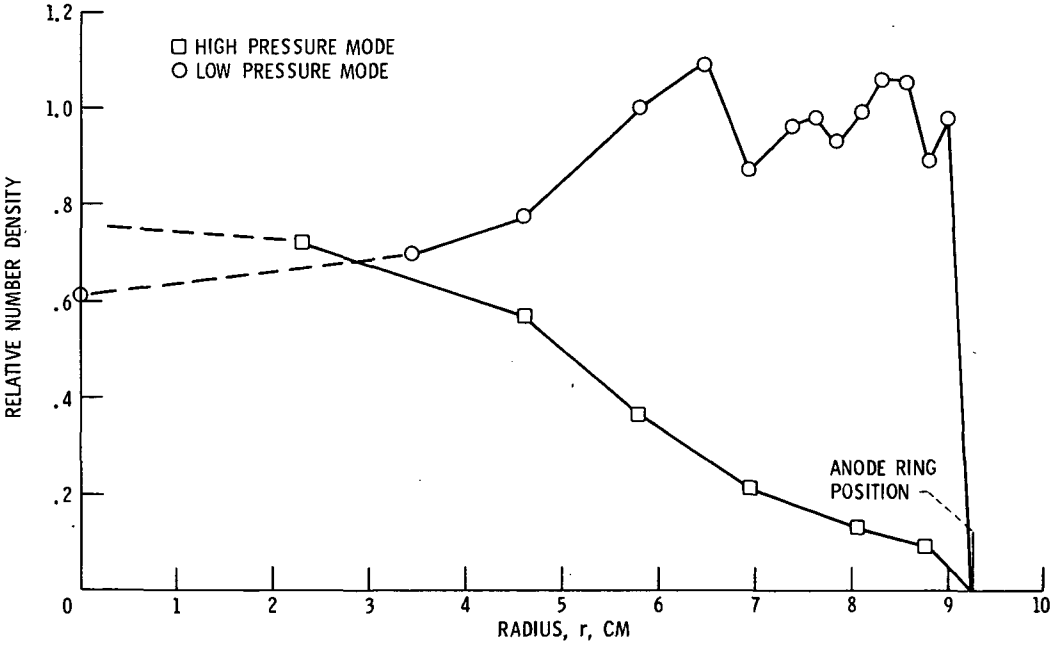

Figure 16. - Radial profiles of relative electron number density for the two operating modes of the discharge.

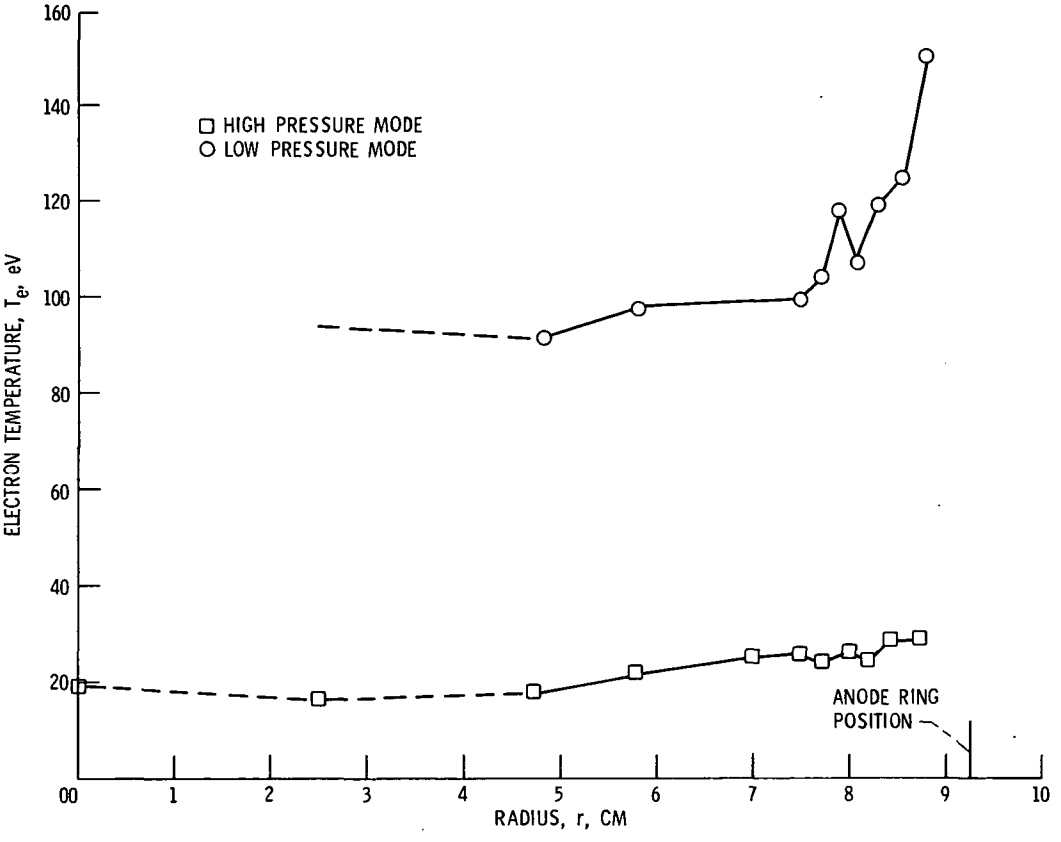

Figure 17. - Radial profile of the electron temperature for the two operating modes of the discharge.

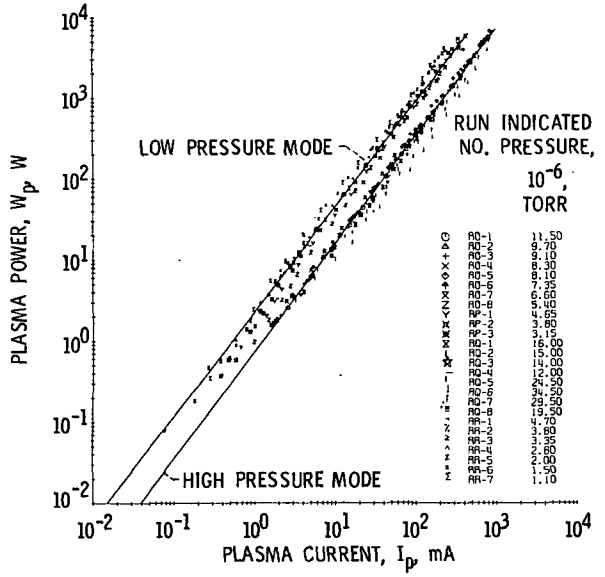

Figure 18. - The dc power flowing to the plasma, W_p, as a function of the anode current, I_p, for a population of data (not that shown in figure 17) taken at a fixed magnetic field of 2.39 T and at various pressures. The data fall into two distinct groups, corresponding to the high and low pressure modes of operation.

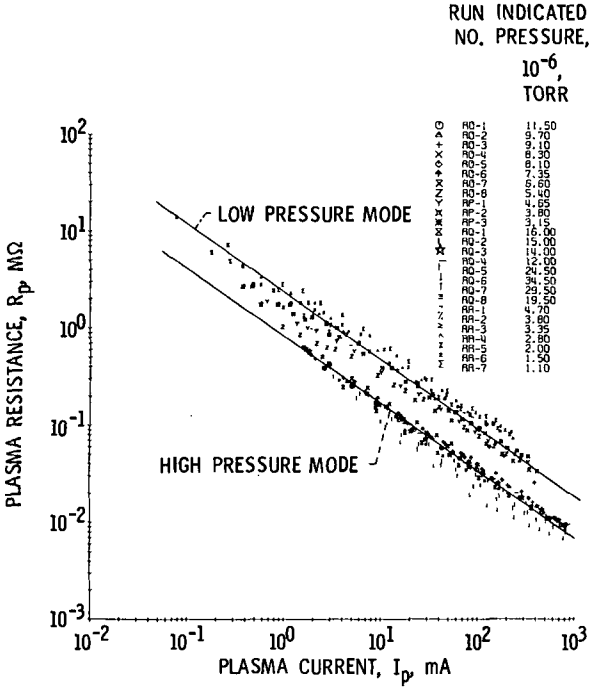

Figure 19. - The dc plasma resistance, $R_p = V_a/I_p$, as a function of the current flowing to the plasma, I_p, for the same data population shown in figure 18. The data fall into two groups, corresponding to the high and low pressure modes of operation.